

The nonlinear growth of surface-tension-driven instabilities of a thin annular film

By MARK JOHNSON¹, ROGER D. KAMM¹, LEE WING HO¹,
ASCHER SHAPIRO¹ AND T. J. PEDLEY²

¹ Department of Mechanical Engineering, Massachusetts Institute of Technology,
Cambridge, MA 02139, USA

² Department of Applied Mathematical Studies, The University of Leeds, Leeds LS2 9JT, UK

(Received 15 August 1990 and in revised form 26 March 1991)

The stability and initial growth rate of disturbances on an annular film lining a cylindrical tube have been the focus of several previous works. The further development of these disturbances as they grow to form stable unduloids or liquid bridges is investigated by means of a thin-film integral model. The model is compared both with perturbation theories for early times, and a numerical solution of the exact equations (NEKTON) for later times. The thin-film model gave results that were in good agreement with solutions of the exact equations. The results show that linear perturbation theory can be used to give good estimates of the times for unduloid and liquid bridge formation. The success of the model derives from the dominant influence of narrow draining regions that feed into the growing unduloid, and these regions remain essentially one-dimensional throughout the growth of the instability.

The model is used to analyse the evolution of the liquid layer lining the small airways of the lung during a single breath. The timescales for formation of unduloids and liquid bridges are found to be short enough for the liquid layer to be in a virtually quasi-equilibrium state throughout the breathing cycle. This conclusion is only tentative, however, because the model assumes that the surface tension of the airway liquid lining does not change with changes in interfacial area despite the known presence of pulmonary surfactant.

1. Introduction

It was first demonstrated by Rayleigh (1879) that a cylindrical column of fluid is unstable to wavelengths (λ) that are longer than the circumference of the cylinder ($2\pi a$). Later he found (Rayleigh 1902) that a modification of this analysis yields the same stability criterion for an annular coating of liquid on the inside of a small tube where a is now taken to be the inner film radius. In this case, the instability eventually leads to one of two different, stable configurations: an unduloid or a liquid bridge, depending on the volume of fluid present (Everett & Haynes 1972). Such thin-film instabilities can have both biological and industrial importance. In the lung where the airway walls are coated with a thin liquid layer that thickens as lung volume falls, a thin-film instability may be responsible for the fact that small airways close during deflation (Frazer & Khoshnood 1979; Kamm & Schroter 1989). Such airway closure isolates a volume of 'trapped' gas in the lung periphery and ultimately limits the amount of gas that can be expired. Surface-tension-induced instabilities have also been studied in the context of two-phase flow in porous media

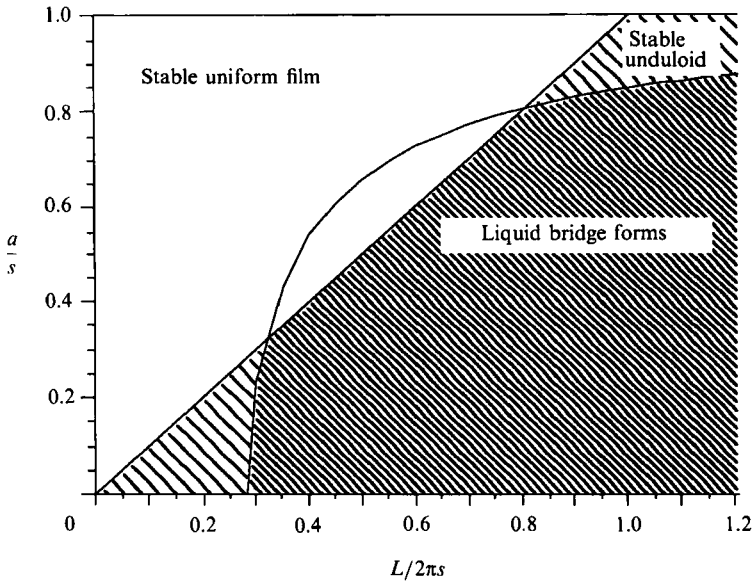


FIGURE 1. Regimes of stability of a uniform film, an unduloid and a liquid bridge as a function a/s (the ratio of film inner radius to tube inner radius) and $L/2\pi s$ for a finite-length tube (length L). The straight line is the stability curve based on Rayleigh's criterion, while the curved line is determined by the minimum volume of fluid required for a liquid bridge to form ($V_c = 5.6 s^3$; Kamm & Schroter 1989).

(Hammond 1983): when water is used to displace oil, a thin film of oil is often left behind; the amount of oil remaining and its subsequent dynamics may affect secondary and tertiary oil recovery.

The thermodynamic stability of a thin film of fluid lining the inside of a cylindrical tube of circular cross-section has been well-characterized along with that of the unduloids and liquid bridges that might form from this uniform thin film (Everett & Haynes 1972). While the thin uniform film is unstable for $\lambda > 2\pi a$, not all wavelengths may be considered as realizable perturbations. Specifically, the admissible wavelengths in tubes of finite length L are constrained to have $\lambda \leq L$, so that proper boundary conditions can be met at the ends of the tube. Figure 1 shows the different regimes that characterize the stability of a liquid film lining the inside of a finite-length tube. It should be noted that the criterion given for liquid bridge formation is valid only if a single lobe forms; multiple lobes can form if $L > 4\pi a$ thus averting collapse of the film into a liquid bridge.

The timescales associated with the irreversible transformation to a new equilibrium state have not yet been completely explored. Furthermore, the parameter that characterizes the transition from viscous-dominated flow to inertial flow has not been firmly established. Goren (1962) examined the initial growth stages of an instability of a uniform liquid film, applying linear perturbation theory to the axisymmetric Navier-Stokes equations. His work implies timescales associated with viscous-dominated flow of $\mu a_0/\sigma$, and inertia-dominated flow of $(\rho a_0^3/\sigma)^{1/2}$, where μ is the fluid viscosity, a_0 is the initial, inner radius of the liquid film, σ is the surface tension of the liquid relative to the fluid in the centre of the tube (e.g. air) and ρ is the density of the liquid. Goren also identified a dimensionless parameter, the ratio of the inertial forces to the viscous forces, multiplied by the ratio of the surface tension forces to the viscous forces, $\rho a_0 \sigma/\mu^2$, which purportedly characterized the flow.

Hammond (1983) extended Goren's work to examine nonlinear distortions of thin films in the regime of viscous-dominated flow. He showed that the viscous timescale is better characterized as $(\mu a/\sigma)(a/h_0)^3$, where $h_0 = s - a_0$ is the initial film thickness, and he pointed out that the effective Reynolds number characterizing the flow would be smaller than the parameter identified by Goren. Hammond's results indicated that, following the initial period of growth characterized by linear perturbation theory, the growth rate was relatively independent of the wavelength of the perturbation. Because of the thin-film assumption, however, Hammond could only speculate on whether the growing instability might eventually lead to the formation of an unduloid or a liquid bridge and was unable to predict the time required to reach a new stable configuration. Gauglitz & Radke (1988) extended Hammond's model by using a more accurate approximation for the surface-tension boundary condition; this improved model did show formation of a liquid bridge under some conditions. Similar studies have been conducted on the breakage of cylindrical columns of liquid using lubrication approximations (Bogy 1979).

In the present study, we extend the work of Hammond and Gauglitz & Radke using integral methods to consider thin films in which inertial effects are admitted and to determine the timescales characterizing formation of unduloids and liquid bridges. The results are compared to the exact solution of Goren in the initial stages of growth and to numerical solutions of the full Navier–Stokes equations for the later times. Finally, we use the thin-film model to characterize the timescales associated with formation of liquid bridges from fluid lining the walls of the terminal bronchi in the lung.

2. The equations of motion

The equations describing the dynamics of the surface-tension-driven flow include the continuity equation (1), the Navier–Stokes equations (2), a kinematic free-surface condition (3), a surface-tension boundary condition setting the normal pressure jump at the free surface (4) and the appropriate boundary conditions on velocity (5).

Our goal in this work is to consider the thin-film limit of these equations, and to determine to what extent the resulting equations can be used as an adequate approximation for thicker films. In the limit of a thin film, the standard boundary-layer or long-wavelength approximation can be made with the result that the radial pressure gradient is negligible compared with its longitudinal variation. Further assuming that $h_0 \ll \lambda$, the viscous terms can be simplified. The resulting equations are

$$\frac{\partial(ru)}{\partial r} + \frac{\partial(rw)}{\partial z} = 0, \quad (1)$$

$$\rho \frac{\partial w}{\partial t} + \rho u \frac{\partial w}{\partial r} + \rho w \frac{\partial w}{\partial z} = -\frac{dP}{dz} + \frac{\mu}{r} \frac{\partial}{\partial r} \left(r \frac{\partial w}{\partial r} \right), \quad (2)$$

$$u|_{r=a} = \frac{\partial a}{\partial t} + w \frac{\partial a}{\partial z}, \quad (3)$$

$$P(z, t) = \frac{\sigma}{s} \left\{ 1 - \frac{h}{s} - s \frac{\partial^2 h}{\partial z^2} \right\}, \quad (4)$$

$$w|_{r=s} = u|_{r=s} = 0; \quad \frac{\partial w}{\partial r} \Big|_{r=a} = 0, \quad (5)$$

where u and w are the radial and axial velocities. The equation of the axisymmetric film surface is taken to be $r = a(z, t)$ in cylindrical coordinates (r, z) ; t is the time.

Equation (4) is the thin-film limit of the surface-tension boundary condition as used by Hammond (1983). While this is an approximation to the full surface-tension equation that is correct in the thin-film limit, it does not properly represent the surface shape for large deformations or for thicker films. In particular, it does not permit non-cylindrical equilibrium shapes of large amplitude, such as the unduloids calculated by Everett & Haynes (1972), nor does it accurately represent the way in which surface tension modifies the film collapse when the instability leads to liquid bridge formation. We therefore replace (4) with the full equation, as follows:

$$P(z, t) = \sigma \left\{ -\frac{\gamma}{a} + \frac{\partial}{\partial z} \left(\gamma \frac{\partial a}{\partial z} \right) \right\} \quad \text{where} \quad \gamma = \left\{ 1 + \left[\frac{\partial a}{\partial z} \right]^2 \right\}^{-\frac{1}{2}}. \quad (6)$$

The resulting model is not strictly 'rational', since we retain the thin-film approximation in the fluid dynamic equations (1)–(3), but it is now accurate for static equilibrium and, as we shall see, not very inaccurate for dynamic states. Other investigators have also incorporated the full curvature term into integral analyses for film flows at moderate Reynolds numbers on plane boundaries (Ruschak 1978; Khesghi 1989).

The equations of motion are now integrated radially across the film. If $w(r, z, t)$ is written as the product of the radially averaged velocity $\bar{w}(z, t)$ and the velocity profile $f(r, z, t)$,

$$w(r, z, t) = \bar{w}(z, t) f(r, z, t),$$

the equations of motion become

$$\frac{\partial a^2}{\partial t} = \frac{\partial}{\partial z} \{ \bar{w}(s^2 - a^2) \}, \quad (7)$$

$$\frac{\partial}{\partial t} [\bar{w}(s^2 - a^2)/2] + \frac{\partial}{\partial z} \left[\bar{w}^2 \int_a^s f^2 r \, dr \right] = -\frac{1}{\rho} \frac{\partial P}{\partial z} \frac{s^2 - a^2}{2} + \frac{\mu}{\rho} s \bar{w} \left. \frac{\partial f}{\partial r} \right|_{r=s}, \quad (8)$$

where $P(z, t)$ is defined by (6).

In the limit of inviscid flow, $f = 1$, while for inertia-free flow with $h \ll \lambda$, $f = \frac{3}{2}\eta(2 - \eta)$ where $\eta = (s - r)/(s - a)$. We substitute the inviscid value of f into the convective term of (8) while using the inertia-free value for the viscous term. This approach is plausible and can be shown to be correct in the appropriate limits but will obviously introduce error when inertial and viscous effects are comparable. We will evaluate the magnitude of this error by comparing with perturbation solutions of the governing equations for several cases.

With these approximations, and using (7), equation (8) becomes

$$\frac{s^2 - a^2}{2} \frac{\partial \bar{w}}{\partial t} + \frac{3\mu s \bar{w}}{\rho(s - a)} = -\frac{s^2 - a^2}{2} \frac{\partial}{\partial z} \left(\frac{\bar{w}^2}{2} + \frac{P}{\rho} \right). \quad (9)$$

3. Linear perturbation theory

Goren's (1962) analysis provides values for the initial growth rate of a surface-tension-driven instability of a cylindrical film. Here we compare his results to the growth rates predicted by (9) to examine the validity of this equation.

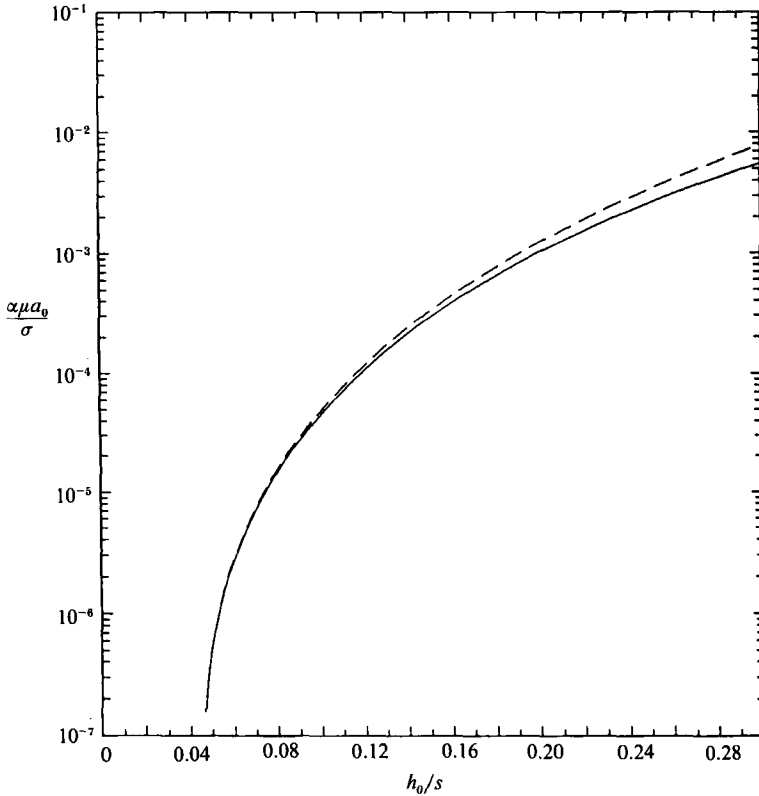


FIGURE 2. The non-dimensional initial growth rate of a perturbation of a thin film ($\lambda/s = 6$) as a function of film thickness (h_0/s) for inertia-free flow. The solid line is from the exact theory of Goren (1962) and the dotted line is from the current model (equation (11)).

We introduce perturbations of the form

$$a = a_0(1 + \epsilon e^{at+2\pi z/\lambda}),$$

$$\bar{w} = \epsilon \nu e^{at+2\pi z/\lambda}$$

to (6), (7) and (9). These perturbations are introduced simultaneously and are consistent (at lowest order) with the equations of motion. Keeping only terms to first order in ϵ , and choosing the coefficient ν for compatibility with (7), a dimensionless growth rate is found to be

$$\frac{\alpha}{\sigma/\mu a_0} = -\frac{1}{G} + \frac{1}{G} \left\{ 1 + \frac{G(\lambda^{*2} - 1)[(s/a_0) - 1]^3[(s/a_0) + 1]}{3\lambda^{*4}} \right\}^{\frac{1}{2}}, \tag{10}$$

where $G = 2\rho\sigma(s - a_0)^2/(3\mu^2 a_0)$ and $\lambda^* = \lambda/(2\pi a_0)$.

In the limit $G \rightarrow 0$ (for constant film dimensions), (10) reduces to

$$\frac{\alpha}{\sigma/\mu a_0} = \frac{(\lambda^{*2} - 1)[(s/a_0) - 1]^2[(s/a_0)^2 - 1]}{6\lambda^{*4}}. \tag{11}$$

Figure 2 compares this with Goren's perturbation solution to the exact equations; the thin-film integral model gives growth rates indistinguishable from the exact solution for $h_0/s < 0.1$ and is a good approximation for $h_0/s < 0.2$. Recall here that $\lambda^* = \lambda/(2\pi a_0)$ and $h_0 = s - a_0$.

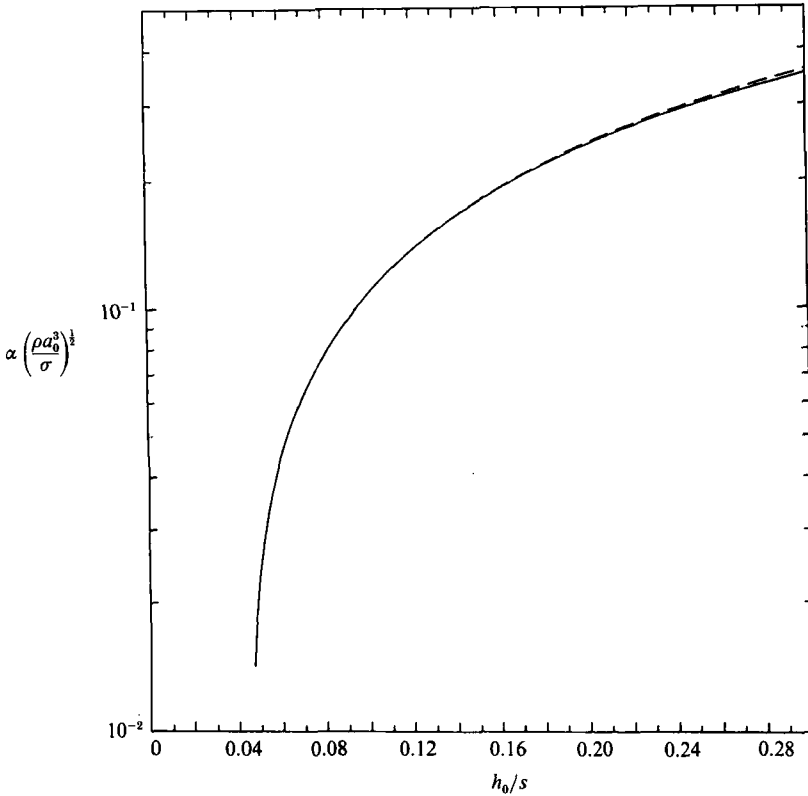


FIGURE 3. The non-dimensional initial growth rate of a perturbation of a thin film ($\lambda/s = 6$) as a function of film thickness (h_0/s) for inviscid flow. The solid line is from the exact theory of Goren (1962) while the dashed line is from the current model (equation (12)).

For the limit $G \rightarrow \infty$, (10) can be rearranged as :

$$\alpha \left(\frac{\rho a_0^3}{\sigma} \right)^{\frac{1}{2}} = \left\{ \frac{(\lambda^{*2} - 1)[(s/\alpha_0)^2 - 1]}{2\lambda^{*4}} \right\}^{\frac{1}{2}}. \tag{12}$$

Figure 3 shows that this is in excellent agreement with Goren’s exact solution.

By taking the ratio of the temporal inertial forces to the viscous forces in (9), and using (10), we can find the effective Reynolds number characterizing the flow. Using (12) to determine α in the inertial limit, and considering thin films, we find that

$$Re \equiv \left(\frac{\rho a_0 \sigma}{9\mu^2} \right)^{\frac{1}{2}} \left(\frac{h_0}{a_0} \right)^{2.5} \left(\frac{\lambda^{*2} - 1}{\lambda^{*4}} \right)^{\frac{1}{2}}. \tag{13}$$

Note that as $\lambda^* \rightarrow 1$, $Re \rightarrow 0$ reflecting the approach toward stability. In the viscous limit, α is given by (11). Then the ratio of temporal inertial forces to viscous forces in (9) becomes, interestingly enough, the square of the expression in (13).

One approximation of concern in deriving (9) was the use of a parabolic velocity profile to estimate the viscous terms while using a flat velocity profile for the inertial terms. While correct in the two limits, this approximation introduces error in the vicinity of $Re = 1$, due to the existence of a developing Stokes layer. Figure 4 shows

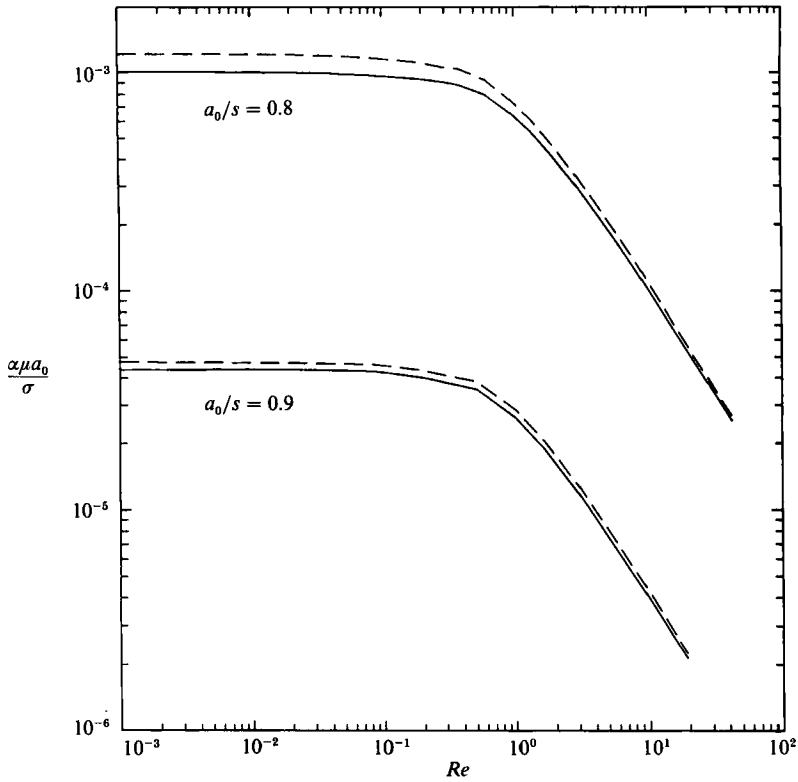


FIGURE 4. The non-dimensional initial growth rate of a perturbation of a thin film ($\lambda/s = 6$) as a function of Reynolds number (as defined by equation (13)) for $a_0/s = 0.8$ and 0.9 . The solid line is from the theory of Goren while the dashed line is from equation (10).

α as a function of Re for $a_0/s = 0.8$ and 0.9 comparing the predictions of (10) to Goren's exact solution. For small values of Re , α is constant as would be expected in the viscous-dominated regime; in the neighbourhood of $Re = 1$, α decreases and approaches the inertial solution as $Re \rightarrow \infty$. The difference between the solutions in the neighbourhood of $Re = 1$ are smaller than those at the viscous limit; this suggests that the error associated with these approximations in velocity profile are not serious, at least in the initial stages of growth of the instability.

4. The numerical model

To model the further development of the instability, past its initial stages characterized by linear perturbation theory, we solved (6), (7) and (9) numerically. Temporal derivatives were modelled using a third-order Adams-Bashforth scheme. All terms were treated explicitly with the exception of the velocity in the viscous term, which was treated implicitly. Defining,

$$g_1 = \frac{\partial}{\partial z} \{ \bar{w}(s^2 - a^2) \}, \quad g_2 = - \frac{\partial}{\partial z} \left(\bar{w}^2 + \frac{P}{\rho} \right) \quad (14)$$

and

$$H(g(t)) = \frac{23}{12}g(t) - \frac{16}{12}g(t - \Delta t) + \frac{5}{12}g(t - 2\Delta t),$$

we find that

$$\frac{a^2(t + \Delta t) - a^2(t)}{\Delta t} = H(g_1(t)) \quad (15)$$

and

$$\frac{\bar{w}(t + \Delta t) - \bar{w}(t)}{\Delta t} + \frac{6\mu s \bar{w}(t + \Delta t)}{\rho(s - a(t))(s^2 - a(t)^2)} = H(g_2(t)). \quad (16)$$

Spatial derivatives were determined using a central-differencing scheme. Image nodes were used at the two boundaries defined such that $\partial a / \partial z$, $\partial P / \partial z$ and $\partial w / \partial z$ were all zero there. Pressure was calculated using an alternative form of (6), namely

$$P(z, t) = -\sigma \left\{ \frac{\gamma}{a} - \gamma^3 \frac{\partial^2 a}{\partial z^2} \right\}. \quad (17)$$

Use of the Courant criterion for numerical stability was not straightforward, as the wave speed associated with film radius change is wavelength dependent. In fact, the limiting wave speed was due to the wavelength associated with the spatial discretization. An alternative method of determining the criterion for numerical stability was derived recognizing the parabolic character of the inertial limit of (6), (7) and (9). After dropping the viscous and nonlinear terms from (9), (6) is substituted into (9). The resulting expression is then differentiated with respect to z while (7) is differentiated with respect to t . Eliminating the common cross-differentiated term and keeping only the most rapidly varying terms, we find

$$\frac{\partial^2 a}{\partial t^2} \approx -\frac{(s^2 - a^2)\sigma}{2\rho a} \left[\frac{1}{a^2} \frac{\partial^2 a}{\partial z^2} + \frac{\partial^4 a}{\partial z^4} \right].$$

If we consider only the highest-order spatial derivative, the stability criterion becomes

$$\frac{\Delta t^2}{\rho a_0^3 / \sigma} < \frac{1}{2} \frac{[\Delta z / a_0]^4}{(s / a_0)^2 - 1}.$$

This condition was used to set Δt with a spatial discretization, Δz , of $L/80$ (smaller step sizes did not yield a significant change in the result).

The initial condition used was a small perturbation of the inner film radius. This did not lead to immediate exponential growth because of the nature of the perturbation: Goren (1962) considered a perturbation in all parameters simultaneously using the stream function to guarantee compatibility; since we initially perturbed only the film thickness, a period of adjustment was necessary until all parameters exhibited exponential growth.

Multiple timescales were observed depending on the number of wavelengths introduced into the initial conditions. Random perturbations were used which led to wavelength selection among modes compatible with the boundary conditions while incommensurate modes appeared to be involved in an energy cascade wherein energy was transferred from the incommensurate wavelengths to those meeting (or approximately meeting) the boundary conditions. In general, this led to a smoothing of the initial disturbance.

To investigate further the timescales associated with the development of the instability of the liquid films, we chose to follow the evolution of a single wavelength: the most unstable mode of linear theory (Goren 1962) that was compatible with the boundary conditions (i.e. $n\lambda = L$ where n is an integer). We followed the evolution in time for cases in which the liquid film was stable ($\lambda < 2\pi a$) or unstable ($\lambda > 2\pi a$). In the former case, the film smoothly approached (low Re) or 'sloshed' around (high Re) the equilibrium position until frictional forces damped out its motion; in the latter case ($\lambda > 2\pi a$), the disturbance grew until either an unduloid or a liquid bridge formed.

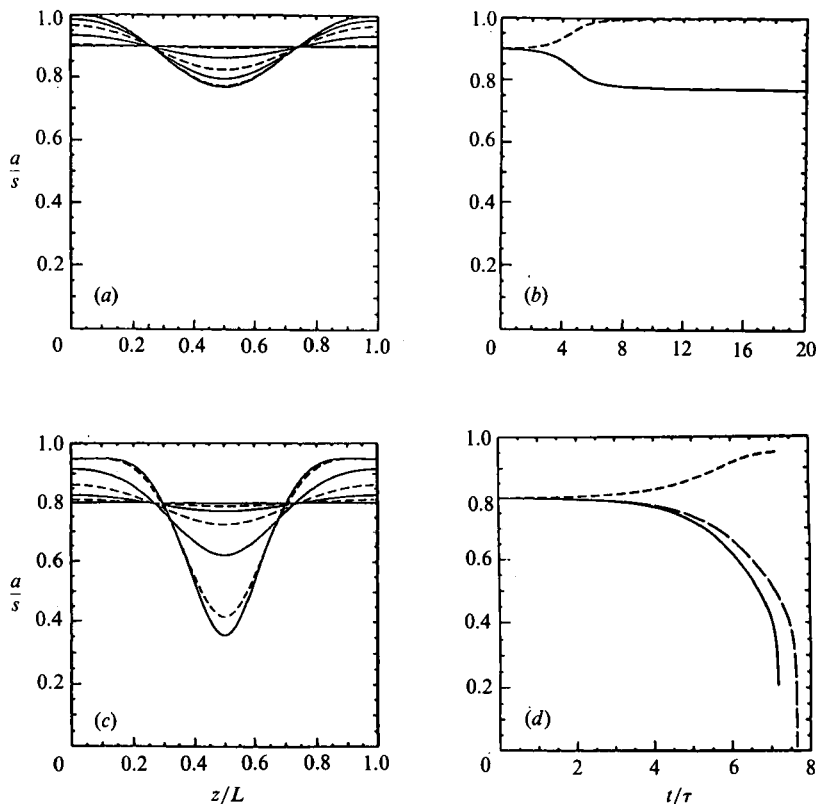


FIGURE 5. Typical results from the quasi-one-dimensional numerical model. (a, b) Formation of a stable unduloid: $a_0/s = 0.9$, $\lambda^* = 1.061$, $Re = 0.060$: (a) profile of the film at various timesteps: 0, 2, 4, 5, 6, 10 and 20τ ; (b) position of the centre of the film (solid line) and the edge of the film (dashed line) as a function of dimensionless time. (c, d) Formation of a liquid bridge: $a_0/s = 0.8$, $\lambda^* = 1.194$, $Re = 0.64$: (c) profile of the film at various timesteps: 0, 3, 4, 5, 6, 7 and 7.1τ ; (d) position of the centre of the film (solid line) and the edge of the film (dashed line) as a function of dimensionless time; also shown is the NEKTON prediction (long-dashed line) for the position of the centre of the film.

Figure 5 shows typical results for the evolution of an instability in which the uniform liquid film either proceeds to a stable unduloid (figure 5a, b), or collapses into a liquid bridge (figure 5c, d). Note the ever-accelerating character when the liquid bridge is formed. Note also the formation of the narrow draining regions at the periphery of the film; the dynamics in these regions control the rate of unduloid formation (Hammond 1983).

4.1. Timescales characterizing film dynamics

For unstable films, several timescales can be considered. There is first the time that characterizes the initial exponential growth of the instability: $\delta(t) = \delta(0) \exp(t/\tau)$. This timescale can be predicted using linear perturbation theory ($\tau = 1/\alpha$). As the disturbance grows, nonlinear effects become important and their effects on timescales need to be evaluated. An unstable film may undergo transition to a stable unduloid or to a liquid bridge and we consider these cases separately.

In the case of transition to a liquid bridge, the disturbance grows until the liquid film bridges across the tube. We define a timescale τ_1 equal to the time for the liquid

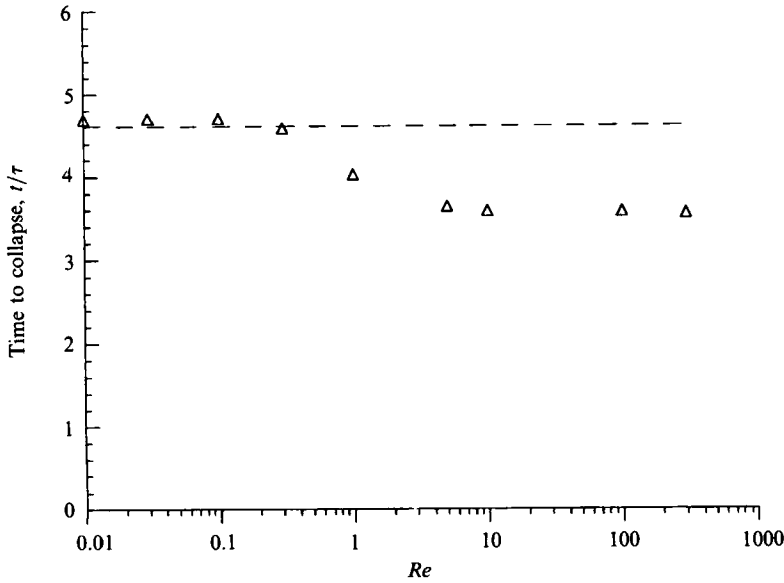


FIGURE 6. Time (τ_1) for liquid bridge to form as a function of Re ; $\lambda^* = 1.194$, $\alpha_0/s = 0.8$. Dashed lines are predictions from linear perturbation theory.

bridge to form from an initial perturbation of 1% of the film inner radius. Thus, if the initial disturbance is $\delta(0)\alpha_0$, the total time required for liquid bridge formation would be the time required for the disturbance to grow to 1% of the film inner radius plus the nonlinear bridge formation time: $\ln(0.01/\delta(0))\tau + \tau_1$.

Using the numerical model we determined the timescales for growth of the instabilities leading from a thin uniform film to a liquid bridge. We compared these with the timescales that would be predicted by extrapolating the linearized exponential growth results. Figure 6 shows the results from the numerical model and the predictions of the linearized perturbation theory. The timescales are expressed as multiples of $\tau = 1/\alpha$ as determined from (10).

The case of transition to a stable unduloid is necessarily more complicated. Following the linear growth stage of the disturbance, there is a timescale associated with nonlinear growth (τ_2) that is analogous to the timescale τ_1 ; however, there are further timescales that characterize the motions of the film as it approaches its new equilibrium position. These timescales are considerably longer since they characterize the draining of the thinning regions into the stable unduloid. This draining process can be further complicated by the temporary formation of multiply-lobed unduloids. These occur when the wavelength of the instability is less than that required for permanent formation of multiple-lobe unduloids ($\lambda > 4\pi a$), and thus the smaller lobe must ultimately drain into the larger lobe.

Numerical simulations for films that form unduloids show that, as in the case of liquid bridge formation, the timescale predicted by linearized growth theory gives useful estimates for the time required to form the unduloid. However, the multiplicity of timescales that describe the formation of an unduloid make it difficult to determine τ_2 precisely, and thus we do not present detailed numerical results here.

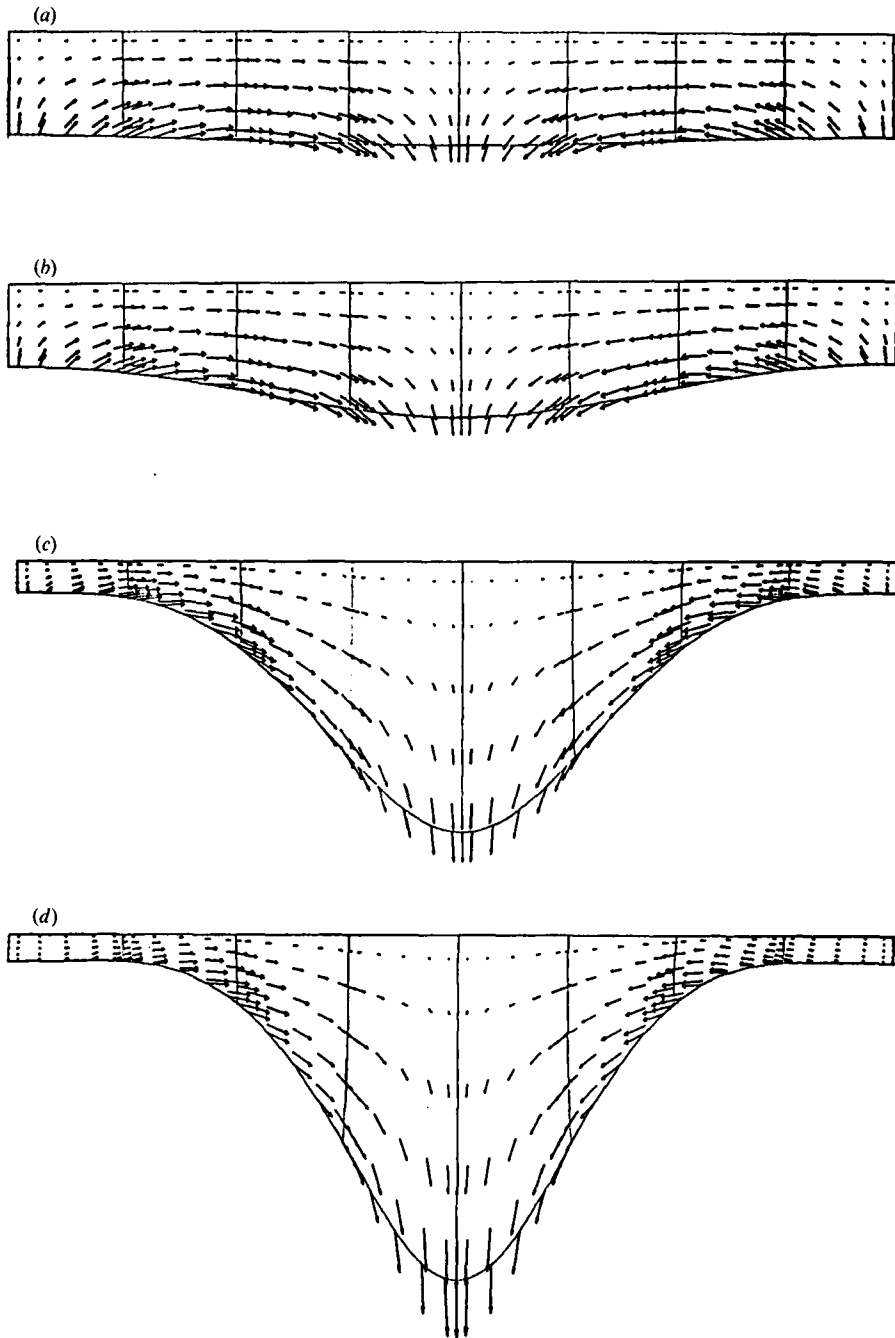


FIGURE 7. The velocity vectors (arrows) in the film, as determined by numerical solution of the exact equations, at four times during the formation of the liquid bridge ($\alpha_0/s = 0.8$, $\lambda^* = 1.194$, $Re = 0.64$). The boundary of each domain shown is the shape of the film at that particular time. Note that the axial scale has been reduced four-fold relative to the radial scale. (a) 0.002 s, Maximum velocity vector 0.13 cm/s; (b) 0.02 s, 0.72 cm/s; (c) 0.04 s, 1.87 cm/s; (d) 0.044 s (0.002 s before film collapse); 2.54 cm/s.

5. Full numerical simulation

As described above, perturbation methods have allowed us to validate the quasi-one-dimensional model, even for relatively thick films ($a_0/s > 0.8$) but only for the initial growth rates. To evaluate the model at later times when significant nonlinear effects become important, we compared a full numerical simulation of the Navier–Stokes equations with the quasi-one-dimensional numerical model. For the numerical simulation, we used a commercially available spectral element code, `NEKTON`, in a form that allows for moving free surfaces (Ho 1989). We considered a relatively thick film ($a_0/s = 0.8$) that proceeded to form a liquid bridge and chose a value for Re such that the inertial and viscous effects would be comparable. This combination was viewed as a stringent test of the model and one that typified conditions encountered in the small airways of the lung (Kamm & Schroter 1989).

Spectral-element methods (Patera 1984; Rønquist 1988; Maday & Patera 1989) are high-order weighted-residual techniques for partial differential equations that combine the high accuracy of p-type spectral techniques (convergence through increased order: Gottlieb & Orszag 1977) with the geometric flexibility of h-type finite-element methods (convergence through increased elemental decomposition: Girault & Raviart 1986; Carey & Oden 1986). In the spatial discretization using spectral elements, the computational domain is subdivided into subdomains or macro-elements, and the dependent and independent variables are approximated by high-order tensor-product polynomial expansions within the subdomains. In the spectral-element formulation for free-surface flows (Ho & Patera 1990*a, b*), the full viscous stress tensor is used for imposition of the surface-tension boundary condition and an arbitrary-Lagrangian–Eulerian description (Ho & Patera 1990*a*) is employed for accurate tracking of all moving boundaries. An elliptic mesh-velocity solver is used in conjunction with this description to accommodate moderately large deformation. Variational projection operators and Gauss numerical quadrature are used to generate the discrete equations, which are efficiently solved by iterative procedures. In the time integration of the governing equations, maximally stable semi-implicit time-stepping formulae are developed (Ho 1989) to decouple the free-surface evolution from all other flow variables in the interior of the fluid.

The particular case considered was one in which $Re = 0.31$ and $\lambda^* = 1.194$. Figure 5(*d*) shows the radial position of the axial midpoint of the film inner radius as a function of time for both the `NEKTON` simulation and for the thin-film model. Even for this relatively thick film and the significant changes in film shape, the quasi-one-dimensional model gives a reasonable correspondence with the spectral calculation.

Figure 7 shows the velocity distribution in the film at four different times. Figure 8 shows the pressure distribution in the film near the end of the collapse process. Note that the pressure is nearly constant within the large unduloid (indicating near equilibrium conditions) while the largest pressure variation occurs in the thin draining regions of the film where the pressure is largely independent of r .

6. Discussion

Our motivation for the current study was to determine the extent to which a thin-film approximation can capture the essential aspects of surface-tension-driven flows occurring within an annular film lining the inside of a small tube, in order to justify the use of similar models to investigate closure in the pulmonary airways. The results indicate that for the cases studied ($a_0/s > 0.8$, $L/s < 4\pi$), the thin-film model gives

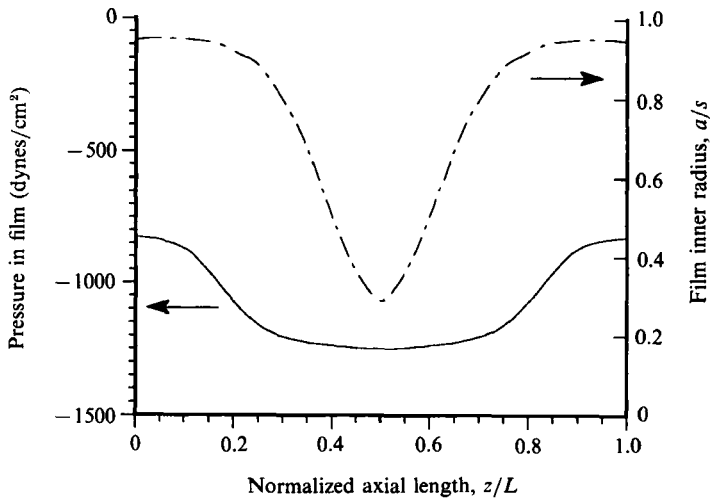


FIGURE 8. Pressure distribution in (solid) and shape of (dot-dashed) the film, as determined by numerical solution of the exact equations, in the late stage ($t = 0.0445$ s) of the formation of the liquid bridge ($a_0/s = 0.8$, $\lambda^* = 1.194$, $Re = 0.64$).

a good approximation to results determined by more precise calculations. This is particularly relevant as the calculations necessary to use the thin-film model are much less complicated than those required to solve the full Navier–Stokes equation. As an example, while a typical calculation such as that considered in §5 required only 15 min of CPU time using the thin-film model (on a VAX 11/750), the same calculation required the equivalent of 350 h of CPU time using the NEKTON code.

The primary reasons for the success of the thin-film model can be seen in figures 7 and 8. While the model fails to capture the detailed dynamics of flow within the forming unduloid, the bulk of the pressure drop driving the flow occurs in the narrow draining regions that feed into the growing unduloid. In these regions, the velocity and pressure distributions are indeed nearly one-dimensional. The quasi-one-dimensional approach was found to be valid until the very final stages of liquid bridge formation, at which time the pressure distribution became fully two-dimensional.

Goren (1964) presented a model in which it was assumed that the film shape passes through a series of quasi-equilibrium forms that minimize the surface area for a given ratio of minimal to maximal film radius subject to the constraint of constant volume. The predicted shapes were unduloids connected by cylindrical link regions, similar to those shown in figure 5(a, c), especially in the later stages of collapse. Comparison between Goren's predicted shapes and the results of the thin-film model showed good agreement although the draining regions were not strictly cylindrical in the thin-film model owing to the axial pressure gradient in this region.

The thin-film model predicts timescales that are smaller than those predicted by more precise calculations. This is probably due to the neglect of the radial pressure gradient and velocity component (in the dynamic equations) that will, in all cases, tend to slow down the instability. The thin-film model was surprisingly accurate in the limit of inviscid flows.

Equations (10)–(12) indicate that the timescale associated with growth of the instability should depend on the wavelength of the perturbation, a reasonable result given the surface-tension boundary condition. However, Hammond's numerical

results (for longer times where nonlinear effects become important) indicated that the timescale for the instability to develop was only weakly dependent on wavelength. This is presumably due to a second interesting finding of Hammond's, namely that the wavelength ultimately dominating the instability process was always close to $2\pi a$, corresponding to $\lambda^* = 1$. As $\lambda^* \rightarrow 1$, equation (10) indicates that $\alpha \rightarrow 0$, or conversely, that the timescale for growth of the instability approaches ∞ . Thus, we would expect a variety of timescales during the growth of the instability. The initial stages of the instability would be dominated by the least-stable wavelength of linear perturbation theory ($\lambda^* = 1.404$ for a thin film) and the timescale of $\tau = 1/\alpha$ is predicted for the initial growth stage of a thin film. Then as the disturbance grows, the dominant wavelength will approach $\lambda^* = 1$ and the timescale will increase. Our results are consistent with this prediction in that in all cases (viscous dominated or inertia dominated), when the liquid film underwent a transition to an unduloid, the resulting wavelength was always close to $\lambda^* = 1$, regardless of the perturbation wavelength; furthermore, when the film underwent a transition to an unduloid, the timescales were always considerably longer than those predicted by the linear perturbation theory.

Our work also identified a 'Reynolds number' that characterizes the transition from viscous- to inertia-dominated regimes (equation (13)). This dimensionless parameter is a function not only of film thickness (as suggested by the work of Hammond) but also of wavelength; furthermore this parameter indicates that the flow always becomes viscous dominated as λ^* approaches 1.

Finally, we examined the timescales associated with the formation of unduloids and liquid bridges. We found that the timescales characterizing the initial growth of the instability (equations (10)–(12)) could be used for an accurate prediction of the time required for liquid bridge formation and gave useful estimates for the time associated with unduloid formation. The success of the thin-film model in characterizing the timescales for liquid bridge formation was primarily due to the fraction of the formation time in which the film remained thin and one-dimensional, as indicated by the pressure and velocity profiles. Only in the very latest stages of collapse did nonlinear effects become prominent as the film thickened and approached collapse. Thus, while the nonlinear terms modify the detailed dynamics of these surface-tension-driven flows, they do not alter the fundamental timescales as characterized by linear perturbation theory.

6.1. *Application to the lung*

Airway closure in the lung periphery can be readily demonstrated by a number of physiological tests and is thought to be responsible for the phenomenon of 'gas trapping' (Macklem 1971). Although widely acknowledged to occur, the mechanisms producing airway closure have not yet been clearly elucidated. Previous studies have suggested that airway closure might occur as a result of an instability of the liquid layer in the small pulmonary airways that thickens as lung volume falls (Frazer & Khoshnood 1979; Kamm & Schroter 1989). For this to be true, however, the timescale for the formation of a liquid bridge clearly must be comparable with or smaller than the breathing period and thus a comparison of timescales would be of interest.

The smallest non-alveolated airways of the human lung (the terminal bronchioles) have a diameter (at full lung inflation) of approximately 0.05 cm and a length of 0.15 cm (Weibel 1963); the liquid lining has been estimated to have a surface tension of approximately 0.02 N/m and a viscosity of 10^{-3} N s/m² (Kamm & Schroter 1989).

The thickness of the liquid lining in these airways is not well-known and in any case will change with the state of lung inflation; the thickness is thought to be 10 μm or less at maximal inflation (Weibel 1963). Thus, $L/2\pi s = 0.955$ and $a_0/s = 0.96$; figure 1 shows that this film will undergo a transition to a stable unduloid.

During expiration, as the diameter and length of the airways decrease, the thickness of the liquid film will increase provided that there is little movement of liquid either into or out of neighbouring airways or via the airway epithelium. Figure 1 indicates that when a/s reaches about 0.8, a liquid bridge will form. Using the given parameters, we find $Re = 0.31$ and $\lambda^* = 1.061$ (neglecting the change in s); this is the case considered in figure 5(c, d). The timescale $\tau = 1/\alpha$ is found from equation (10) to be 0.0089 s; thus, the results in figure 5 indicate that liquid bridge formation will occur in approximately 65 ms, much faster than the normal breathing process. Furthermore, since unduloid formation occurs on a timescale similar to that of liquid bridge formation, these results suggest that the liquid films in the airways exhibit equilibrium configurations (as determined by figure 1) during normal breathing. This conclusion should be valid for both normal and high-frequency ventilation.

These conclusions should be viewed as tentative, however, since the model described herein assumes that the surface tension of the airway liquid lining does not change with changes in interfacial area despite the known presence of pulmonary surfactant. Surfactant would tend to slow the film instability owing both to the effect of surface tension gradients at the interface and to a reduction in the surface-tension-induced pressure gradient within the liquid layer. These effects are currently being evaluated.

We would like to thank Professor Tony Patera of MIT for his many suggestions and help on this project and acknowledge the support of the National Heart, Lung and Blood Institute (HL33009) and the Freeman Foundation.

REFERENCES

- BOGY, D. B. 1979 Drop formation in a circular liquid jet. *Ann. Rev. Fluid Mech.* **11**, 207.
- CAREY, G. F. & ODEN, J. T. 1986 *Finite Elements: Fluid Mechanics*, vol. VI. Prentice-Hall.
- EVERETT, D. H. & HAYNES, J. M. 1972 Model studies of capillary condensation: I. Cylindrical pore model with zero contact angle. *J. Colloid Interface Sci.* **38**, 125.
- FRAZER, D. G. & KHOSHNOOD, B. 1979 A model of the gas trapping mechanism in excised lungs. *Proc. 7th New England Bioengng Conf.*, vol. 9, p. 482.
- GAUGLITZ, P. A. & RADKE, C. J. 1988 An extended evolution equation for liquid film breakup in cylindrical capillaries. *Chem. Engng Sci.* **43**, 1457.
- GIRAULT, V. & RAVIART, P. A. 1986 *Finite Element Approximation of the Navier–Stokes Equations*. Springer.
- GOREN, S. L. 1962 The stability of an annular thread of fluid. *J. Fluid Mech.* **12**, 309.
- GOREN, S. L. 1964 The shape of a thread of liquid undergoing break-up. *J. Colloid Sci.* **19**, 81.
- GOTTLIEB, D. & ORSZAG, S. A. 1977 *Numerical Methods of Spectral Methods: Theory and Applications*. SIAM.
- HAMMOND, P. S. 1983 Nonlinear adjustment of a thin annular film of viscous fluid surrounding a thread of another within a circular cylindrical pipe. *J. Fluid Mech.* **137**, 363.
- HO, L. W. 1989 A Legendre spectral element method for simulation of unsteady incompressible viscous free-surface flows. Ph.D. thesis, MIT.
- HO, L. W. & PATERA, A. T. 1990a A Legendre spectral element method for stimulation of unsteady incompressible viscous free-surface flows. *Comput. Meth. Appl. Mech. Engng* **80**, 355–366.

- HO, L. W. & PATERA, A. T. 1990*b* Variational formulation of three-dimensional viscous free-surface flows: natural imposition of surface tension boundary conditions. *Intl J. Numer. Meth. Fluids* (to appear).
- KAMM, R. D. & SCHROTER, R. C. 1989 Is airway closure caused by a liquid film instability? *Respir. Physiol.* **75**, 141.
- KHESHGI, H. S. 1989 Profile equations for film flows at moderate Reynolds numbers. *AIChE J.* **35**, 1719.
- MACKLEM, P. T. 1971 Airway obstruction and collateral ventilation. *Physiol. Rev.* **51**, 368–385.
- MADAY, Y. & PATERA, A. T. 1989 Spectral element methods for the Navier–Stokes equations. In *State-of-the-art Surveys on Computational Mechanics* (ed. J. T. Oden & A. K. Norr). ASME.
- PATERA, A. T. 1984 A spectral element method for fluid dynamics; laminar flow in a channel expansion. *J. Comput. Phys.* **54**, 468.
- RAYLEIGH, LORD 1879 On the capillary phenomena of jets. Appendix I. *Proc. R. Soc. Lond. A* **29**, 71.
- RAYLEIGH, LORD 1902 On the instability of cylindrical fluid surfaces. *Scientific Papers*, vol. 3, pp. 594–596. Cambridge University Press.
- RÖNQVIST, E. M. 1988 Optimal spectral element methods for the unsteady three-dimensional incompressible Navier–Stokes equations, Ph.D. thesis, MIT.
- RUSCHAK, K. J. 1978 Flow of a falling film into a pool. *AIChE J.* **24**, 705.
- WEIBEL, E. R. 1963 *Morphometry of the Human Lung*. Springer.